International Journal of Thermodynamics (IJoT)
ISSN 1301-9724 / e-ISSN 2146-1511
www.ijoticat.com

Vol. 17 (No. 4), pp. 202-208, 2014
doi: 10.5541/ijot.530
Published online: December 01, 2014

Numerical Study of Entropy Generation in the Flameless Oxidation Using Large Eddy Simulation Model and OpenFOAM Software

S. M. Mousavi, J. Abolfazli-Esfahani* and M. Yazdi-Mamaghani

Center of Excellence on Modelling and Control Systems (CEMCS) & Mechanical Engineering Department, Ferdowsi University of Mashhad, Mashhad 91775-1111, Iran
* abolfazl@um.ac.ir

Abstract

This paper employs large eddy simulation (LES) to investigate non-premixed flameless oxidation occurring in the IFRF furnace with varying fuel-injection angle. In order to model radiation and combustion using OpenFOAM software, finite volume discrete ordinate model and partially stirred reactor are applied whereas the detailed mechanism GRI-2.11 is undertaken represent chemistry reactions. The obtained results are compared with the experimental measurements of Mancini's et al. After ensuring the accuracy of the LES method, the combustion characteristics are examined when using different fuel injection angles into the combustion chamber. The results explain using fuel injection with an angle into the combustion chamber, the net rate of reaction and entropy generation increases.

Keywords: *Flameless oxidation; large eddy simulation; injection angle; entropy generation*

1. Introduction

The energy production and its consumption has always been one of the human beings main concerns. Nowadays, regarding the restriction of the fossil energy resources and their environmental impacts, the researchers are trying to find appropriate solutions for energy saving and reduction of combustion pollutant emissions. One of the approaches is the application of flameless oxidation technology (FLOX). FLOX technology was initially developed to minimize NO_x emissions produced in industrial furnaces using high temperature preheated air [1]. In FLOX technology, the input temperature of reactants is higher, while the temperature rise during combustion is lower, than the self-ignition temperature of the reactant mixture [2]. This new combustion technology is also named "Moderate or Intense Low-oxygen Dilution (MILD)" and "high temperature air combustion (HiTAC)".

In the last two decades or so, this type of combustion has examined experimentally and numerically. Weber et al. [3] investigated experimentally the MILD combustion of different fuels, i.e., natural gas (NG), light fuel oil (LFO), heavy fuel oil (HFO), and coal. In their investigation, the oxidizer includes 20% oxygen, 60% nitrogen, 14% water vapor, and 6% carbon dioxide at 1300 oC. They found that the MILD combustion process of light oil was similar to that of natural gas to a great deal while the MILD combustions of heavy fuel oil and coal were significantly different always with visible flames. Lille et al. [4] experimentally studied HiTAC combustion of a single fuel jet of Gasol (> 95% of propane). Their studies revealed that the combustion of Gasol in hot and oxygen depleted flue gases appeared to be so stable and complete. They also found that reduced oxygen concentration in the flue gases increased the flame size and lift-off distance but decreased luminosity and visibility. Their results display that the HiTAC flame becomes bluish first then appeared to be non-visible at the oxygen concentration below 15% in the oxidizer. Their measurement of reactant concentrations inside the combustion chamber confirmed that the HiTAC flame volume and surface were much larger than conventional combustion. Very low emissions of exhaust NO_x and CO were measured in their experiment. Colorado et al. [5] investigated experimentally performance of FLOX using biogas and natural gas. They found that, in both cases, NO_x and CO emissions were very low, lower than 3 ppm and 16 ppm, respectively. When the system was fueled by biogas, the efficiency was 2% lower than in the case of natural gas combustion, and a minor reduction of the temperature field was found.

There are a great number of relevant numerical studies available in the literature. Christo and Dally [6] tested several models for MILD combustion and found that the eddy dissipation concept (EDC) model with a detailed kinetic scheme is the best. Recently, HiTAC has been also simulated for coal [7, 8]. Mardani and Tabejamaat [9] studied the effect of hydrogen on hydrogen methane turbulent non-premixed flame under MILD combustion regime by using CFD. They found that the reduction of hydrogen in fuel leads to enlarge the reaction zone volume, and to reduce the mixture fraction and strain rate. Moreover, the radial spreading of flame decreases by addition of hydrogen to the fuel mixture. Mardani et al. [10] studied numerically the importance of molecular diffusion versus turbulent transport in the MILD combustion mode. Their results demonstrate that the molecular diffusion in MILD combustion cannot be ignored in comparison with the turbulent transport. They also observed that the inclusion method of molecular diffusion in combustion modeling has a considerable effect on the accuracy of numerical modeling of MILD combustion. Their results showed that by decreasing the jet Reynolds number and the oxygen concentration in the airflow or increasing H_2 in the fuel mixture, the influence of molecular diffusion on MILD combustion increases. Mi et al. [11] investigated the

influence of the injection momentum rate of premixed air and fuel on the MILD combustion in a recuperative combustion chamber by using the computational fluid dynamic (CFD). They found that the flue gas recirculation plays an essential role in establishing the premixed MILD combustion. They also found that there is a critical momentum rate of the fuel-air mixture, under which the MILD combustion does not happen. Moreover, the momentum rate of the fuel-air mixture has a less significant influence on conventional global combustion than on MILD combustion. Parente et al. [12] presented a simplified modeling approach for the prediction of NO_x formation in MILD combustion at low temperatures with high concentration of H_2 in the fuel stream for a semi-industrial combustion chamber. They compared CFD predictions with the experimental data. Their examination indicated that the proposed CFD model has the capability to provide a satisfactory description of the system over the wide range of operating conditions. Also they found that reasonable predictions of NO_x formation are achieved only when an accurate characterization of the temperature field taking into account of all the relevant NO_x formation routes of the investigated operating conditions. For instance, the inclusion of non-conventional NO_x formation routes such as N_2O is crucial for characterizing the pollutant emissions from the combustion at low temperatures and with hydrogen added fuel. Coelho and Peters [13], Ihme and See [14], and Afarin and Tabejamaat [15] confirmed the large eddy simulation (LES) for modeling the FLOX combustion.

In present study, FLOX technology is simulated using OpenFOAM software. In this context, LES and partially stirred reactor (PaSR) are applied in order to model turbulence and the combustion, respectively. The flow field is discretized using the volume method and PISO algorithm coupled the pressure and velocity fields. The results are compared with the available experimental data [16]. The good agreement between the present numerical and published experimental data [16] validates the used method and confirms its ability to model the similar cases. After verifying the results of simulation, the effects of using injection with an angle into the combustion chamber on net rate of reaction and entropy generation are examined.

2. Mathematical model

The governing equations including the Favre-averaged form of continuity, momentum, energy, species conservation, and LES equations are solved in order to simulate the flow field numerically [17]. The so-called Top-hat filter [18] is applied for divides the quantities into filtered and unfiltered quantities. The Favre-averaged and Smagorinsky model [18] are used for averaging of the filtered quantities in Navier-Stokes equations and modeling the unfiltered quantities, respectively. In this study, C++ library OpenFOAM is used for numerical simulation. Here the flow solver is based on the PISO algorithm [19]. The DRM-22 which is a reduced version of the GRI1.2, models the chemical kinetics [19]; it consists of 22 species and 104 reversible reactions. The time step is about 10^{-6} s, which is reduced to 10^{-8} s when the combustion starts.

2.1 Large eddy simulation

The naturally three dimensional and unsteady turbulent flows are often influenced by strong non-homogeneous effects and rapid transformations which prevent using the isotropic models in simulations. The modified sub-grids methods which can improve LES models are also presented although their usage is confined due to their natural complexity. Therefore new methods for simulating the sub-grids scale (SGS) are in progress. In common methods some models are presented to consider the effects of sub-grids scale in filtered Navier-Stokes equations [20]. LES is more common than the other models. In this model at first large scales should be solved with energy which is given to them. For this purpose the effect of the small scales which are waste, should be considered in energy balance. In LES model, the filter is used to separate the large scales from small ones [21]. Therefore all variables like f are divided into two parts, grid scale (GS) and sub-grid. In other words $f=\bar{f}+\acute{f}$ where $\tilde{f}=\bar{\rho}f/\bar{\rho}$ is sub-grid tension. In variable density flow $\tilde{f}=\bar{\rho}f/\bar{\rho}$ where $f=\tilde{f}+f''$ [21].

By filtering the variables in compressible Navier-stokes equations, the instantaneous filtered equation leads to the following equations. A more detailed discussion can be found in the textbooks by Poinsot and Veynante [22].

$$\frac{\partial \bar{\rho}}{\partial t}+\frac{\partial}{\partial x_i}.(\rho\tilde{u}_i)=0 \tag{1}$$

$$\frac{\partial \bar{\rho}\tilde{Y_k}}{\partial t}+\frac{\partial}{\partial x_i}\left(\bar{\rho}\tilde{u}_i\tilde{Y_k}\right)= \frac{\partial}{\partial x_i}\left(\left(\mu+\frac{\mu_{SGS}}{Sc_t}\right)\frac{\partial \tilde{Y_k}}{\partial x_i}\right)+\bar{\dot{\omega}} \quad \text{k=1,...,N} \tag{2}$$

$$\frac{\partial \bar{\rho}\tilde{u}_i}{\partial t}+\frac{\partial}{\partial x_i}\left(\bar{\rho}\tilde{u}_i\tilde{u}_j\right)+\frac{\partial \bar{p}}{\partial x_i}=\frac{\partial}{\partial x_i}\left(\overline{\tau_{ij}}+\mu_{SGS}\left(\frac{\partial \tilde{u}_i}{\partial x_j}+\frac{\partial \tilde{u}_i}{\partial x_i}\right)+\frac{\delta_{ij}}{3}T_{kk}\right) \tag{3}$$

$$\frac{\partial \bar{\rho}\tilde{h}}{\partial t}+\frac{\partial}{\partial x_i}\left(\bar{\rho}\tilde{u}_i\tilde{h}\right)=\frac{\overline{Dp}}{Dt}\frac{\partial}{\partial x_i}\left(\left(\frac{\mu}{\mathrm{Pr}}+\frac{\mu_{SGS}}{\mathrm{Pr}_t}\right)\frac{\partial \tilde{h}}{\partial x_i}\right) \tag{4}$$

In the above equations, the symbols ˜ and ¯ indicate filtered Faver and filtered quantities, respectively, and u is the velocity vector, p is the pressure, ρ is the flow density, h is the enthalpy, Y_k is the mass fraction of kth species, an δ is the Kronecker delta. The isentropic contribution, T_{kk}, in equation (which is twice the sub-grid scale turbulent kinetic energy) is unknown and usually absorbed into the filtered pressure. Furthermore, Sc_t and Pr_t are considered as unity. All terms in above equations are closed except the species transport's (Eq. (2)) source term.

Furthermore, the sub-grid scale kinetic energy obtained by,

$$\frac{\partial K_{SGS}}{\partial t}+\frac{\partial \tilde{u}_j K_{SGS}}{\partial x_i}=\frac{\partial}{\partial x_i}\left(\frac{\mu_{SGS}}{\bar{\rho}\,\mathrm{Pr}_t}\frac{\partial K_{SGS}}{\partial x_i}\right)-\tau_{ij}\frac{\partial \tilde{u}_j}{\partial x_i}-\varepsilon_{SGS} \tag{5}$$

The μ_{SGS} is the sub-grid scale viscosity; ε_{SGS} is the sub-grid scale dissipation, τ is the stress tensor which are computed according to the expressions,

$$\mu_{SGS}=\bar{\rho}C_k\sqrt{K_{SGS}}\Delta \tag{6}$$

$$\varepsilon_{SGS}=\frac{C_e K_{SGS}\sqrt{K_{SGS}}}{\Delta} \tag{7}$$

$$\tau_{ij} = -2\frac{\mu_{SGS}}{\bar{\rho}}\bar{S}_{ij} + \frac{2}{3}K_{SGS}\delta_{ij} \tag{8}$$

where C_k and C_e are set to 0.2 and 1.048 in this study. In addition the grid scale rate of stress tensor ($\bar{S}_{ij}$) is defined as following:

$$\bar{S}_{ij} = \frac{1}{2}\left(\frac{\partial \tilde{u}_i}{\partial x_j} + \frac{\partial \tilde{u}_j}{\partial x_i}\right) \tag{9}$$

The DRM-22 which is a reduced version of the GRI1.2, models the chemical kinetics, it consists of 22 species and 104 reversible reactions. Finally reaction mechanism is expressed in Eq. (10).

$$\sum_{i=1}^{N} P'_{ij}\Im_i \underset{k_{b,j}}{\overset{k_{f,j}}{\rightleftharpoons}} \sum_{i=1}^{N} P''_{ij}\Im_i \tag{10}$$

In the above relation, k_{fj} and k_{bj} are the forward and backward rate constants of equilibrium reaction, respectively. Furthermore the filtered species reaction rates are

$$\overline{\dot{\omega}_i} = M_i\left(P''_{ij} - P'_{ij}\right)\overline{\dot{\omega}_j} \tag{11}$$

In which the j[th] reaction rate is:

$$\dot{\omega}_j = k_{f,i}\prod_{i=1}^{N}\left(\rho Y_i\right)^{P'_{ij}} - k_{b,j}\prod_{i=1}^{N}\left(\rho Y_i\right)^{P''_{ij}} \tag{12}$$

where according to Eq. (3), Y_i is the mass fraction of species *i*.

2.2 PaSR method

The turbulence flow is related to the combustion terms using the PaSR method. In PaSR method each computational cell is divided into two parts, reactive and unreactive. In reactive part it is supposed that the participant components in reaction are mixed well which is the main assumption of PSR method. The final mixture consists of both burned and unburned gases as the results of reactive and unreactive parts respectively. The ratio of reactive to unreactive parts in PaSR is calculated as [19],

$$R = \frac{\tau_c}{\tau_c - \tau_{mix}} \tag{13}$$

In the above equation, $\tau_{mix} = C_{mix}\sqrt{\mu_{eff}/\left(\bar{\rho}\varepsilon_{SGS}\right)}$ is mixing time and C_{mix} is equal to one. The value of time step in chemical reaction (τ_c) is determined based on total molar concentration in each computational cell and average of its variations. Based on PaSR model, the rate of molar concentration changes of chemical components is

$$\frac{\partial C^i}{\partial t} = \frac{C_1^i - C_0^i}{\tau_{res}} = \dot{\omega}_i(C_1^i) \tag{14}$$

In this equation, C_1^i and C_0^i are the values of final concentration and initial concentration of species i respectively. Also, residence time (τ_{res}) is equal to time step of solution.

2.3 Entropy generation

The irreversibility in fluid flow is caused by heat transfer and viscosity. Entropy generation in this collection by determining the temperature and velocity profile is considered as below,

$$S''_{gen} = \left(S'''_{gen}\right)_{heat} + \left(S'''_{gen}\right)_{fric} \tag{15}$$

First and second terms of Eq. (15) are associating the heat and friction, correspondingly,

$$\left(S'''_{gen}\right)_{heat} = (\lambda_{eff}/T^2)\cdot \left[\left(\partial T/\partial x\right)^2 + \left(\partial T/\partial y\right)^2 + \left(\partial T/\partial z\right)^2\right] \tag{16}$$

The term due to friction is,

$$\left(S''_{gen}\right)_{fric} = \mu_{eff}/T \cdot \Phi \tag{17}$$

Φ is presented in Eq. (18),

$$\Phi = 2\cdot\left[\left(\frac{\partial u}{\partial x}\right)^2 + \left(\frac{\partial v}{\partial y}\right)^2 + \left(\frac{\partial w}{\partial z}\right)^2\right] + \left(\frac{\partial u}{\partial x} + \frac{\partial v}{\partial y} + \frac{\partial w}{\partial z}\right) \tag{18}$$

According to the Stanciu et al. [23], entropy generation is caused by the heat transfer, friction and by species dispersion especially reaction rate in combustion phenomena. These values can be obtained for species dispersion and reaction rate as below

$$\left(\dot{S}_{gen}^{(\Omega)}\right)_D = \sum_{i=1}^{N}\rho D_{im}\left[\frac{\dot{\omega}_i}{p}\frac{\partial Y_i}{\partial z_\alpha}\frac{\partial p}{\partial z_\alpha} + \frac{\dot{\omega}_i}{Y_i}\frac{\partial Y_i}{\partial z_\alpha}\frac{\partial Y_i}{\partial z_\alpha}\right] > 0 \tag{19}$$

$$\left(\dot{S}_{gen}^{(\Omega)}\right)_{CH} = \frac{\dot{\omega}}{T}\sum_{i=1}^{N}\left(\upsilon'_i - \upsilon''_i\right)\mu_{M,i} > 0 \tag{20}$$

where $\mu_{M,i}$ is molar chemical potential for species *i*, and υ'_i and υ''_i are the stoichiometric coefficients of reactants and products, respectively.

For calculating the entropy generation rate in the whole combustion chamber and in Cartesian coordinates it is presented as,

$$\dot{S}_{gen} = \iiint_V S'''_{gen}dx\cdot dy\cdot dz \tag{21}$$

2.4 Discretization

The discretization scheme with higher order is needed in LES model, because the sub-grid terms covering using leading-order truncation error should be prevented. Totally, sub-grid terms are proportionated with Δ^P such that $4.3 < P$

<2. The filter width (Δ) is usually related to generated grids and also produces the modeled sub-grid scale stresses and flux parameters whereas the their magnitude are equal to $O(|d|^p)$. It should be considered that $/d/$ is magnitude of grid in $\Delta \propto |d|$. In LES model, spectral or pseudo spectral, and high-order finite volume or finite difference methods are used for spatial discretization, and explicit semi-implicit or predictor–corrector methods of at least second-order accuracy are used for time integration. On the other hand LES model does not usually filter for time domain, therefore, it should be solved for those scales in which ($\nabla t < \tau_k$) where ∇t is time step and τ_k is Kolmogorov time scale, Courant number lower than 0.2, and only large scale should be remained.

According to definition of cell average approximation f on the p^{th}-cell, Gauss theory is used to extract the semi discretization equations of LES model.

All the calculations are preceded by utilizing OpenFOAM software and due to entropy generation computation, the numerical cods of C++ is added to OpenFOAM solver. It should be pointed out that the computations are done with getting help from parallel processing center of Ferdowsi University of Mashhad.

3. Geometrical modeling

The combustion chamber which is considered in the present work is shown schematically in Figure 1. The oxidizer was supplied through the central channel with an injection velocity of 80 m/s. The fuel was supplied through two injectors with an injection velocity of 110 m/s. According to Figure 1, the fuel injectors were located 0.28 m away from the combustion chamber centerline. In addition, the diameters of fuel, oxidizer, and outlet nozzle are 0.0273, 0.125, and 0.75 m, respectively. Moreover, the length, width, and height of the combustion chamber are 6.25, 2, and 2 m, individually. The inlet velocity, temperature, and composition of fuel/oxidizer are also illustrated obviously in Table 1 in order to compare the numerical results with the available experimental data [16]. No slip, impenetrable and constant temperature conditions are applied for walls. Additionally the pressure of the outlet is constant and is considered to be 1 atm.

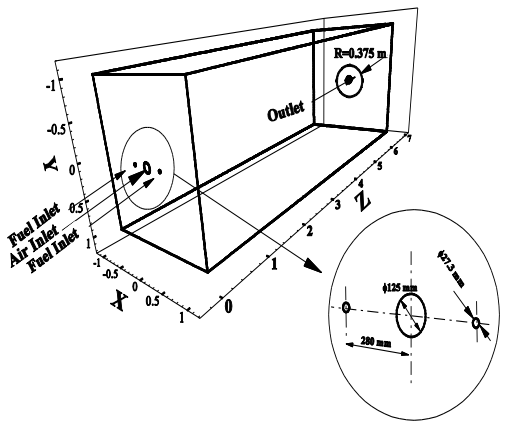

Figure 1. A schematic of the combustion chamber.

Table 1. The input conditions of the simulation [16]

	Velocity ($m.s^{-1}$)	Temperature (K)	Composition %(vol)
Fuel	80	300	CH_4 87.8%, C_2H_6 4.6%, C_3H_8 1.6%, C_4H_{10} 0.5%, N_2 5.5%
Oxidizer	110	1600	wet O_2 19.5%, wet N_2 60%, H_2O 15%, wet CO_2 6%, NO 110 ppm

4. Result and discussion

In order to obtain the optimum number of grids in terms of speed, accuracy of solution, and grid independency, the model has been solved with 10 different sizes of grids, and the results have been reported as an average temperature chart on the central line (Z direction), the mean temperature at the outlet of the combustion chamber and average speed at Z = 3.1 m. According to Figure 2, when the number of the computational cells is more than 3.8×10^6, the results will approximately be constant. Considering this low deviation and the computational costs, grid with 3.8×10^6 cells has been used in this work.

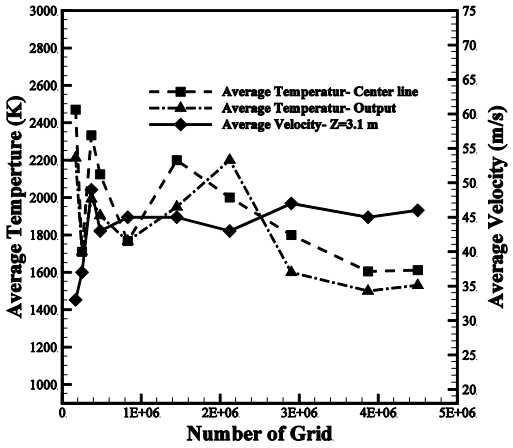

Figure 2. The effect of different cell numbers.

Pope [24] suggested that the simulation of LES model has high accuracy while the ratio of kinetic energy to turbulence-resolution tolerance (α) is more than 80%. Figure 3 indicates the variations of α versus Y in four sections 0.4, 1.4, 3, and 5.5 m from the inlet of the nozzles. It is observed that the amount of α reaches more than 89% in all parts of the surface. Thus, LES model's accuracy for current model stimulation is confirmed.

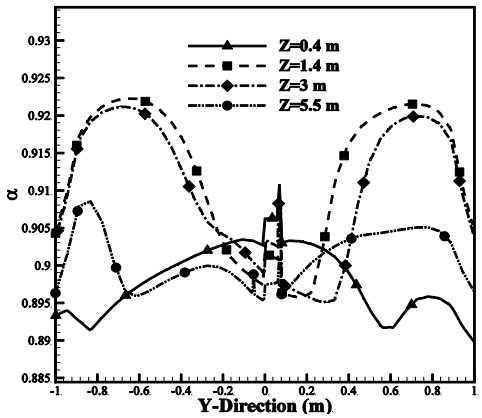

Figure 3. The variations of α versus Y in four sections 0.4, 1.4, 3, and 5.5 m from the inlet of the nozzles.

In order to comparison of PDF model results [16] with results of the present study, Figures 4 and 5 display temperature profile and NO_x emission in Y-direction where z axis is equal to 0.73 m. As it is evident, to compare with experimental data the accuracy of the numerical results of present study is much greater than PDF model [16]. The errors which are appeared in PDF method in most points are caused by inability of this model to predict the local extinction probably. The result shows the ability of LES model to the prediction of the FLOX behavior.

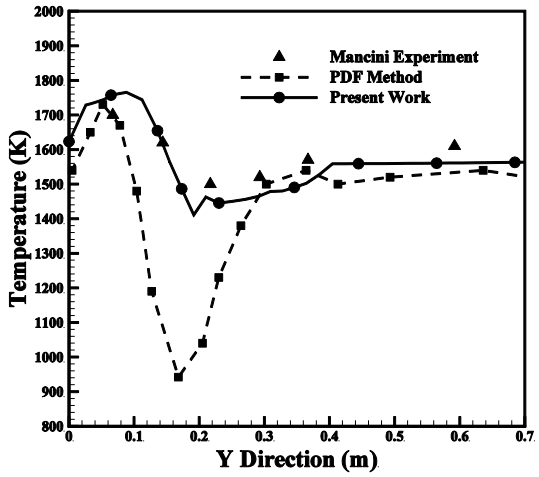

Figure 4. Temperature profile in Y-direction.

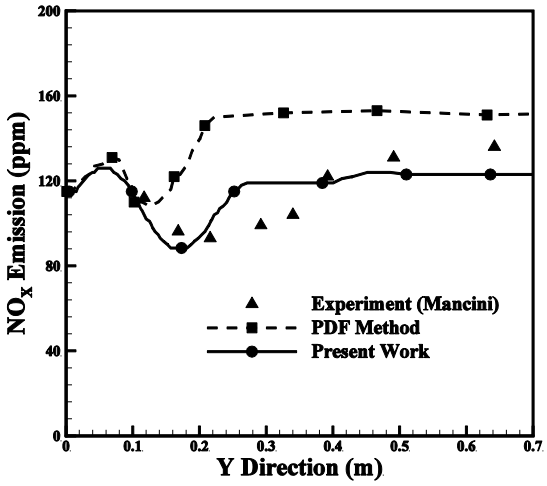

Figure 5. The profile of NO_x emission in Y-direction.

After ensuring the accuracy of the simulation method, the combustion behavior is examined using fuel injection with an angle in the combustion chamber. Then, its impact on location of primary flow collision, distribution of reaction rate, and entropy generation is discussed.

Figures 6 and 7 show the flow path while without chemical reaction for different cases of injection, including direct injection and injection with an angle. The combustion chamber is divided into zone 1 and 2 based on the location of the fuel and oxidizer collision region. As it is seen in Figures 6 and 7, using direct injection lead to happen the flow collision in zone 2, while the fuel injection with angle leads to occur the flow collision in zone 1. Thus, there are more opportunities and time for the mixing of fuel and oxidizer. Additionally, it is clear that, whatever the injection angle increases, the location of mixing flows (fuel and oxidizer) moves closer to the inlet region, and the inlet jets collide more rapidly, which increases turbulence intensity.

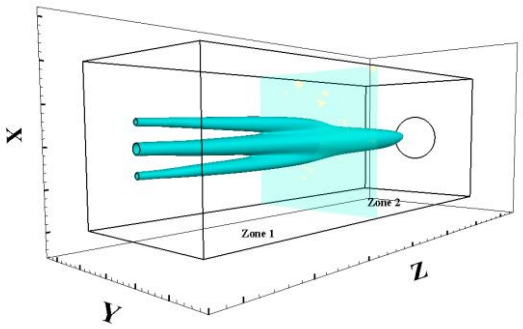

Figure 6. The flow paths of air and fuel in the combustion chamber (direct injection).

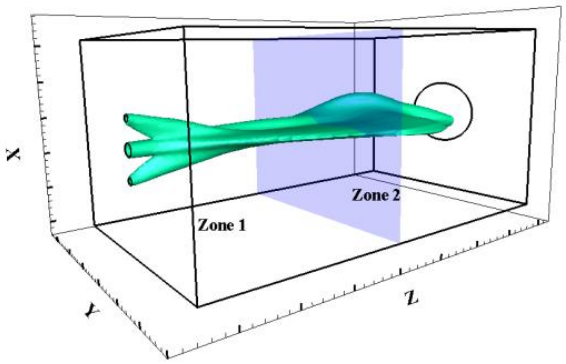

Figure 7. The flow paths of air and fuel in the combustion chamber (injection with an angle).

Figure 8 shows the distribution of reaction rate through the z-direction for different injection angles. According to this figure, using injection with an angle is increased the reaction rate. Attention to Eq. (14), the rate of molar concentration changes of chemical components is dependent on the net rate of reaction, then, applying injection with an angle into the combustion chamber is increased the rate of molar concentration changes of chemical components.

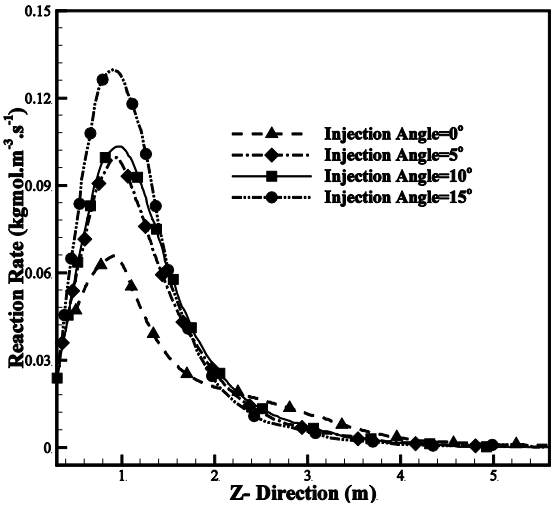

Figure 8. The distribution of reaction rate through the z-direction for different injection angles.

Figure 9 (a-d) indicates the entropy distribution in the combustion chamber for different kinds of fuel injection. In this figure, it can be clearly seen that, applying fuel

injection with an angle increases the entropy generation. Increase in the entropy generation due to the increase in the reaction rate according to Eqs. (19) and (20) is predictable. Additionally, in section (2.3) it is shown that, the entropy generation increases by applying injection with an angle into the combustion chamber for two reasons: increase in the reaction rate and pressure gradients, which are the source of entropy generation.

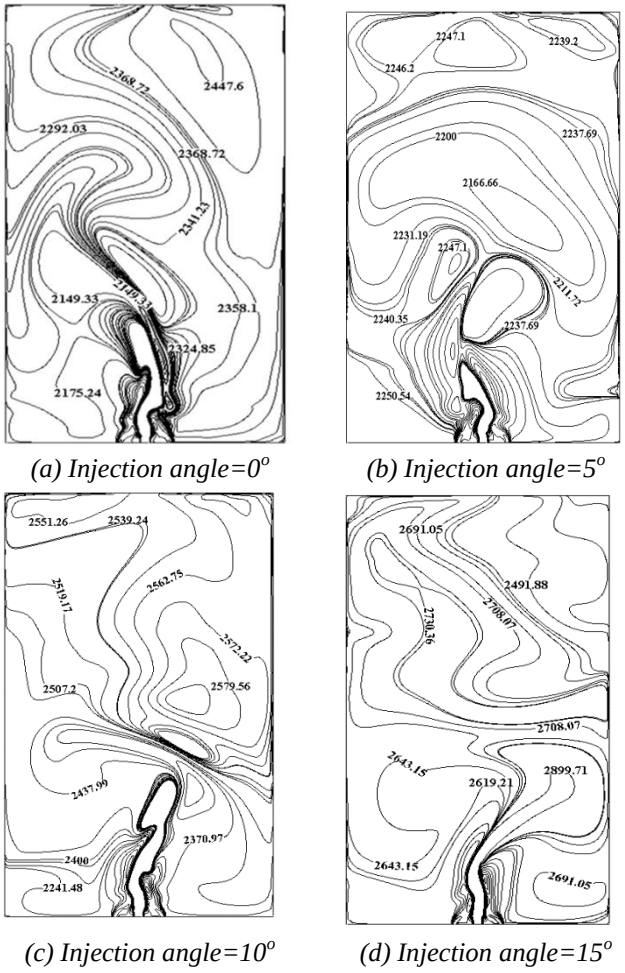

(a) Injection angle=0^o *(b) Injection angle=5^o*

(c) Injection angle=10^o *(d) Injection angle=15^o*

Figure 9. The distribution of entropy generation (horizontal axis=x-coordinate, vertical axis= z-coordinate)

5. Conclusions

In present study, FLOX combustion is simulated using OpenFOAM software. In this context, LES and PaSR are applied in order to model turbulence and the combustion, respectively. The flow field is discretized using the volume method and PISO algorithm coupled the pressure and velocity fields. The good agreement between the present numerical and published experimental data [16] validates the used method and confirms its ability to model the similar cases. After verifying the results of simulation, behavior of combustion is examined using fuel injection with an angle into the combustion chamber. The obtained results are as follows:

- The location of mixing flows (fuel and oxidizer) moves closer to the inlet region,
- Direct injection leads to the mixing process in zone 2, while as the fuel injection with an angle lead to occur the mixing process in both zones, there are more opportunities and time for the mixing of fuel and oxidizer.
- Using fuel injection with an angle into the combustion chamber leads to an increase in the reaction rate,
- Entropy generation increases by applying injection with an angle into the combustion chamber for two increase in the reaction rate and pressure gradients.

References

[1] J. P. Smart and G. S. Riley, "Combustion of coal in a flameless oxidation environment under oxyfuel firing conditions: the reality," *J. Energy Institute*, 85, 131-134, 2012.

[2] A. Cavaliere and M. de Joannon, "Mild Combustion," *Progress in Energy and Combustion Science*, 30, 329-366, 2004.

[3] R. Weber, J. P. Smart, and W. V. Kamp, "On the (MILD) combustion of gaseous, liquid, and solid fuels in high temperature preheated air," *Proceedings of the Combustion Institute*, 30, 2623-2629, 2005.

[4] S. Lille, W. Blasiak, and M. Jewartowski, "Experimental study of the fuel jet combustion in high temperature and low oxygen content exhaust gases," *Energy*, 30, 373-384, 2005.

[5] A. F. Colorado, B. A. Herrera, and A. A. Amell, "Performance of a Flameless combustion furnace using biogas and natural gas," *Bioresource Technology*, 101, 2443-2449, 2010.

[6] F. C. Christo and B. B. Dally, "Modeling turbulent reacting jets issuing into a hot and diluted coflow," *Combustion and Flame*, 142, 117-129, 2005.

[7] J. P. Kim, U. Schnell, G. Scheffknecht, and A. Benim, "Numerical modelling of mild combustion for coal," *Progress in Computational Fluid Dynamics, an International Journal*, 7, 337-346, 2007.

[8] N. Schaffel, M. Mancini, A. Szle¸k, and R. Weber, "Mathematical modeling of MILD combustion of pulverized coal," *Combustion and Flame*, 156, 1771-1784, 2009.

[9] A. Mardani and S. Tabejamaat, "Effect of hydrogen on hydrogen–methane turbulent non-premixed flame under MILD condition," *International J. Hydrogen Energy*, 35, 11324-11331, 2010.

[10] A. Mardani, S. Tabejamaat, and M. Ghamari, "Numerical study of influence of molecular diffusion in the Mild combustion regime," *Combustion Theory and Modelling*, 14, 747-774, 2010.

[11] J. Mi, P. Li, and C. Zheng, "Numerical Simulation of Flameless Premixed Combustion with an Annular Nozzle in a Recuperative Furnace," *Chinese J. Chemical Engineering*, 18, 10-17, 2010.

[12] A. Parente, C. Galletti, and L. Tognotti, "A simplified approach for predicting NO formation in MILD combustion of CH4–H2 mixtures," *Proceedings of the Combustion Institute*, 33, 3343-3350, 2011.

[13] P. J. Coelho and N. Peters, "Unsteady modelling of a piloted methane/air jet flame based on the Eulerian particle flamelet model," *Combustion and Flame*, 124, 444-465, 2001.

[14] M. Ihme and Y. C. See, "LES flamelet modeling of a three-stream MILD combustor: Analysis of flame sensitivity to scalar inflow conditions," *Proceedings of the Combustion Institute*, 33, 1309-1317, 2011.

[15] Y. Afarin and S. Tabejamaat, "The effect of fuel inlet turbulence intensity on H2/CH4 flame structure of MILD combustion using the LES method," *Combustion Theory and Modelling*, 17, 383-410, 2012.

[16] M. Mancini, R. Weber, and U. Bollettini, "Predicting NOx emissions of a burner operated in flameless oxidation mode," *Proceedings of the Combustion Institute*, 29, 1155-1163, 2002.

[17] C. Fureby and G. Tabor, "Mathematical and Physical Constraints on Large-Eddy Simulations," *Theoretical and Computational Fluid Dynamics*, 9, 85-102, 1997.

[18] C. Fureby and F. F. Grinstein, "Large eddy simulation of high-Reynolds-number free and wall-bounded flows," *J. Computational Physics*, 181, 68-97, 2002.

[19] M. Hallaji and K. Mazaheri, "Comparison of LES and RANS in Numerical Simulation of Turbulent Non-Premixed Flame under MILD Combustion Condition," in *7th Mediterranean Combustion Symposium*. *Chia Laguna, Cagliari, Sardinia, Italy, September 11-15, 2011*.

[20] S. Huang and Q. Li, "A new dynamic one-equation subgrid-scale model for large eddy simulations," *International J. Numerical Methods in Engineering*, 81, 835-865, 2010.

[21] M. Chapuis, C. Fureby, E. Fedina, N. Alin, and J. Tegnér, "Les modeling of combustion applications using OpenFOAM," in *ECCOMAS CFD*, 2010, pp. 14-17.

[22] T. Poinsot and D. Veynante, "Theoretical and numerical combustion," Edwards, 2005, pp. 162.

[23] D. Stanciu, D. Isvoranu, M. Marinescu, and Y. Gogus, "Second law analysis of diffusion flames," *Int. J. Appl. Thermodynamics*, 4, 1-18, 2001.

[24] S. B. Pope, "Ten questions concerning the large-eddy simulation of turbulent flows," *New J. Physics*, 6, 35, 2004.